ACS Catalysis

Open Access
This article is licensed under CC-BY 4.0

pubs.acs.org/acscatalysis
Research Article

Electronic and Structural Property Comparison of Iridium-Based OER Nanocatalysts Enabled by *Operando* Ir L_3-Edge X-ray Absorption Spectroscopy

Marianne van der Merwe,* Romualdus Enggar Wibowo, Catalina E. Jimenez, Carlos Escudero, Giovanni Agostini, Marcus Bär, and Raul Garcia-Diez*

Cite This: *ACS Catal.* 2024, 14, 16759−16769
Read Online

ACCESS | Metrics & More | Article Recommendations | Supporting Information

ABSTRACT: In this study, we investigate the electronic and structural behavior of a newly developed and of a commercially available Ir-based oxygen evolution reaction (OER) catalyst under relevant conditions employing an *operando* Ir L_3-edge X-ray absorption near-edge structure and extended X-ray absorption fine structure approach. The newly developed Kopernikus P2X amorphous IrO_x/TiO_2 catalyst is compared to the current commercial benchmark catalyst: crystalline IrO_2/TiO_2, Umicore Elyst. Analysis of the redox behavior of the catalysts shows distinct electronic differences between the amorphous and crystalline oxides, with the former exhibiting significant reversible electronic transformations. Employing an equivalent charge transfer approach following Faraday's law of electrolysis, we study the behavior of the catalysts under equivalent OER conditions (chronopotentiometric steps), as opposed to the conventional chronoamperometric approach. This enables the derivation of property−structure relationships under equivalent OER conditions for materials exhibiting distinctly different activities. The P2X IrO_x/TiO_2 catalyst undergoes substantial electronic structure changes, with larger reduction in the Ir−O bond lengths compared to that of the commercial benchmark catalyst. The correlation between electronic states and local geometric information highlights diverse OER pathways, suggesting that the newly developed P2X IrO_x/TiO_2 catalyst and the benchmark IrO_2/TiO_2 commercial catalyst follow mechanisms akin to those of amorphous iridium oxide (am-IrO_x) and rutile-IrO_2, respectively. These results shed light on the intrinsic activities of different iridium oxide-based catalysts and provide crucial insights for enhancing their performances in proton exchange membrane water electrolyzers.

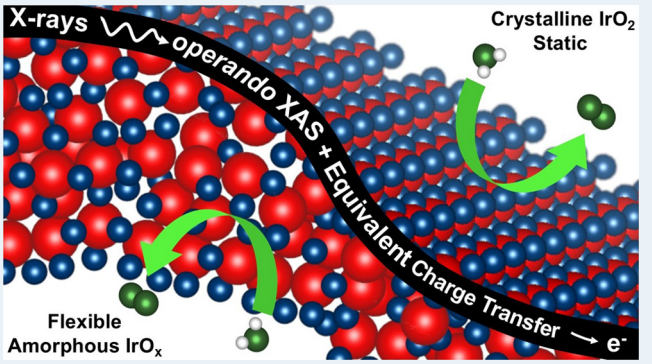

KEYWORDS: *oxygen evolution reaction, Ir-based catalyst, operando Ir L_3-edge X-ray absorption spectroscopy, chronopotentiometry, equivalent charge transfer*

Downloaded via HELMHOLTZ ZENTRUM BERLIN on November 15, 2024 at 12:43:30 (UTC).
See https://pubs.acs.org/sharingguidelines for options on how to legitimately share published articles.

INTRODUCTION

Proton exchange membrane water electrolysis (PEM-WE) is suggested as a key technology essential for advancing hydrogen (H_2)-based energy supply systems, facilitating the storage of surplus energy derived from intermittent renewable energy sources.[1,2] Nevertheless, the harsh conditions inherent to the oxygen evolution reaction (OER) at the anode presents significant challenges, impeding widespread commercialization of this technology. Overcoming this challenge necessitates the development of robust and high-performance anode materials, with iridium-based materials currently representing the state-of-the-art catalyst used in commercial applications.[3]

Considerable efforts have been directed toward designing highly active and highly stable iridium-based anode materials. Notably, reducing the noble metal content has been primary focus, with a target of ~0.05 mg_{Ir}/cm^2 required to realize a global H_2 economy where green-H_2 is produced by PEM-WE technology.[2,4] One approach to enhance iridium utilization while reducing loading involves supporting iridium oxide on support materials like highly stable, nonconductive titanium oxide (TiO_2) or electrically conductive yet less stable antimony-doped tin oxide (ATO).[5,6] Recent findings indicate that a very thin layer of nanostructured IrO_x supported on nonconductive TiO_2 can serve as a highly efficient catalyst when achieving a well-connected network of supported conductive IrOx nanoparticles on the support.[7]

Received: June 17, 2024
Revised: October 1, 2024
Accepted: October 23, 2024
Published: October 30, 2024

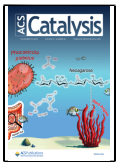

© 2024 The Authors. Published by American Chemical Society

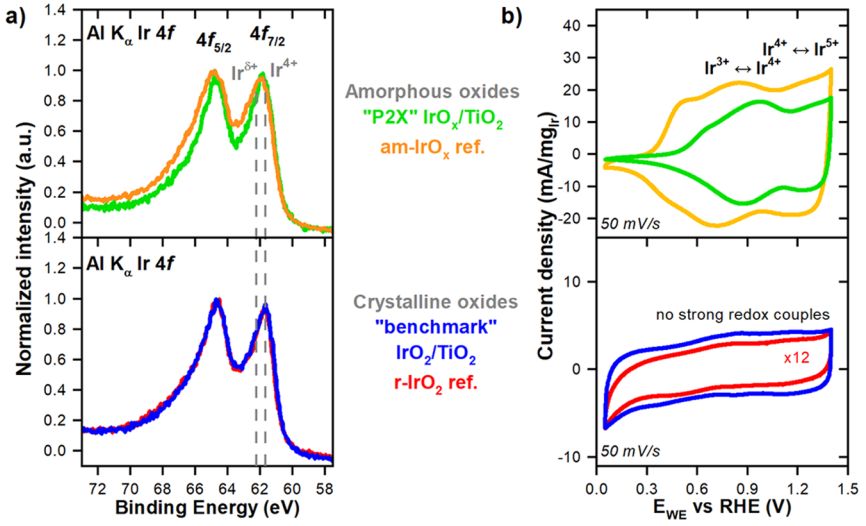

Figure 1. (a) *Ex situ* XPS Ir 4f detailed spectra measured using an Al K_α source (IMFP = 15.5 Å assuming ρ = 11.6 g/cm^3) and (b) cyclic voltammograms (CVs) recorded at 50 mV/s between 0.05 and 1.4 V_{RHE} in 0.5 M H_2SO_4 of the amorphous and crystalline iridium oxides. The top panels show the amorphous oxides: the "P2X" IrO_x/TiO_2 catalyst (30 wt %), in green, and the am-IrO_x reference, in orange. The bottom panels show the crystalline oxides: "benchmark" IrO_2/TiO_2 (Elyst 75), Umicore, in blue, and the r-IrO_2 reference, in red. The Ir 4f spectra are normalized to the maximum of the 4$f_{7/2}$ peak. Vertical dashed lines in (a) indicate the binding energies of the Ir^{4+} and predicted trivalent ($Ir^{\delta+}$) Ir-species. The CVs of the catalysts are shown normalized to the mass of iridium oxide to yield a mass-specific current density. The CV of the r-IrO_2 reference is magnified by ×12.

Within the framework of the Kopernikus P2X project,[8] a highly efficient iridium oxide anode material has been developed in the past years. This material, featuring a thin core−shell layer of amorphous iridium oxide deposited on a high-surface-area nonconductive TiO_2 support—IrO_x/TiO_2 (Heraeus Precious Metals GmbH & Co. KG (HPMG), Deutschland, Germany), hereafter referred to as the "P2X catalyst", boasts a competitively low iridium packing density (~0.5 mg_{Ir}/cm^2, close to the target value of 0.05 mg_{Ir}/cm^2) with a sufficiently high electrical conductivity through a well-interconnected network of IrO_x on the TiO_2 support.[9,10] This results in a continued high OER performance even after long duration (3700 h) PEM stack testing.[9,10] In contrast, the current commercial benchmark OER catalyst consists of a crystalline iridium oxide (IrO_2) deposited on electrically nonconductive titanium oxide (TiO_2) support, featuring a 75 wt % iridium loading (Elyst Ir75 from Umicore, Germany), hereafter referred to as the "benchmark catalyst". This catalyst exhibits a thick iridium core−shell, necessitating a high iridium packing density (~2 mg_{Ir}/cm^2, factor 40 higher than the target value) for optimal membrane electrode assembly performance,[4] which is significantly higher than the long-term target. Recent comparative studies have elucidated significant differences in mass activities and long duration operation profiles between the P2X and commercial benchmark catalysts.[9,10] The enhanced activity of the P2X catalyst has been attributed to the higher intrinsic activity of its amorphous IrO_x species compared to that of the crystalline IrO_2 species of the commercial benchmark catalyst, arising from the different mechanisms governing OER in these distinct iridium oxide species;[11−20] however, confirmation of detailed electronic and structural information on these catalysts under relevant OER conditions is still pending. Our study therefore focuses on investigating the behavior of these iridium oxide-based catalysts under relevant, comparative OER conditions by investigating their electronic and structural properties using *operando* Ir L_3-edge X-ray absorption spectroscopy (XAS).

Recent discourse has raised critiques regarding *operando* XAS investigations on iridium oxide anode materials, highlighting multiple disparities among the various studies concerning factors such as identification/classification of the surface OER active sites and determination of the iridium oxidation states.[21,22] These disparities stem from a lack of uniformity and consistency in methodologies employed, particularly in sample preparation and *operando* electrochemical protocols, posing challenges to the achievement of a comprehensive understanding of the OER mechanisms of crystalline and amorphous iridium oxides, resulting in several pathways proposed through the years.[11−20] Moreover, direct comparisons among studies are often challenging due to the different intrinsic activities of materials such as crystalline and amorphous iridium oxides, the latter exhibiting lower OER overpotentials. These factors hinder a reliable comparison across the studies and the electrocatalysts of structural parameters, like Ir−O bond lengths or the average iridium oxidation state, emphasizing the need for standardized and comprehensive spectro-electrochemical protocols to investigate iridium oxide anode materials under comparable electrochemical conditions.[23,24]

While primarily targeting electrochemists engaged in catalyst development studies, these calls for standardization should extend to the application of *operando* XAS protocols for investigating property−structure relationships. Stepped chronoamperometry (CA) experimental protocols in the redox and OER potential range (between ~0.3 V_{RHE} and ~1.6 V_{RHE}) have been the only approaches in previous *operando* studies.[25−28] While being suitable for exploring the chemical and electronic transformations of a single catalyst, this method falls short of a fair and consistent evaluation when comparing materials with significantly different OER activities (i.e., different rates of O_2 generation under the same applied potential). Given that OER is a 4-electron transfer process, investigations of the electronic transformations of catalysts with different activities should be based on an equivalent

https://doi.org/10.1021/acscatal.4c03562
ACS Catal. 2024, 14, 16759−16769

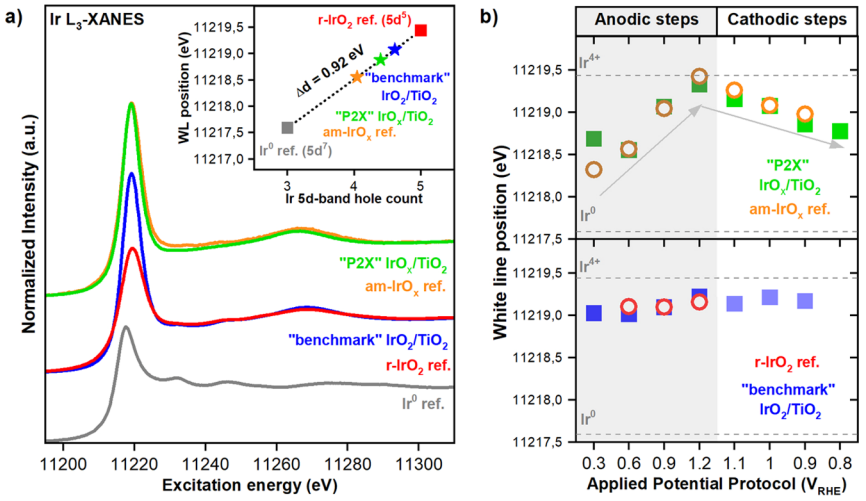

Figure 2. (a) *Ex situ* Ir L_3-edge XANES spectra of the crystalline iridium oxides ("benchmark" 75 wt % IrO_2/TiO_2 in blue and r-IrO_2 reference in red) and the amorphous iridium oxides ("P2X" 30 wt %IrO_x/TiO_2 in green and am-IrO_x reference in orange). The XANES spectrum of metallic iridium (Ir^0) is shown for reference. The inset plot shows the WL position versus the formal Ir 5d-band hole count calibration line utilizing the metallic Ir ($5d^7$) and r-IrO_2 ($5d^5$) reference materials with a slope value of $\Delta d = 0.92$ eV. The interpolated formal Ir 5d-band hole counts of the WL positions of am-IrO_x, commercial benchmark IrO_2/TiO_2, and P2X IrO_x/TiO_2 catalyst at open circuit voltage within the 0.5 M H_2SO_4 electrolyte solution are also shown. (b) *Operando* Ir L_3-edge WL positions of the crystalline oxides (top panel) and amorphous oxides (bottom panel) as a function of the applied potential protocol over the redox couple regime in anodic steps (0.3 V_{RHE} to 1.2 V_{RHE}) and in cathodic steps (1.2 V_{RHE} to 0.8 V_{RHE}) in a 0.5 M H_2SO_4 electrolyte solution. The commercial "benchmark" and P2X catalyst are shown by solid blue and green squares, respectively, and the reference iridium oxides (IrO_2 and am-IrO_x) are shown as open (red and orange) circles. The horizontal dashed lines show the WL positions of the Ir^0 and Ir^{4+} references.

charge transfer approach following Faraday's law of electrolysis ($Q = I{\cdot}t = n{\cdot}F$) using an equivalent current density protocol for the *operando* studies. Equivalent current density is also the standard metric used for evaluating OER activity,[29,30] allowing for the classification and comparison of property−structure relationships in amorphous and crystalline iridium oxides at the same degree of OER electrocatalytic activity.

Consequently, our *operando* XAS investigations of different iridium oxides utilize the approach of chronopotentiometric (CP) steps opposed to chronoamperometric (CA) steps to reveal property−structure relationships under OER relevant conditions, given that the CP approach allows for systematic comparison of "equivalent charge transfer" between catalysts. Well-known rutile-IrO_2 (r-IrO_2) and amorphous iridium oxide (am-IrO_x) reference materials are also included to help relate electrochemical properties with spectroscopic findings and thereby obtain a better understanding of the structure transformation of the newly developed and of the commercial iridium oxide-based OER catalysts. In this study, we investigate both redox potential regions (potentials between +0.3 V_{RHE} and +1.2 V_{RHE}) and the OER regions (potentials >1.23 V_{RHE}) to provide a comprehensive understanding of the catalysts' behavior. Examining these regions allows us to explore the interplay between the catalysts' redox properties and their oxygen evolution activity, offering insights into their performance and stability across a wide range of operational conditions.

RESULTS AND DISCUSSION

Surface Characterization and Electrochemical Behavior of the Amorphous and the Crystalline Iridium Oxide Catalysts. *Ex situ* X-ray photoelectron spectroscopy (XPS) measurements were performed to characterize the initial iridium chemical states of the surface species of the studied iridium oxide-based catalysts (IMFP = 15.5 Å assuming ρ = 11.6 g/cm[3][31]). The Ir 4f spectra (Figure 1a) of the crystalline oxides, including the commercial "benchmark" IrO_2/TiO_2 (Umicore) catalyst and the r-IrO_2 reference catalyst (Sigma-Aldrich), exhibit narrower Ir 4f peaks compared to their amorphous iridium oxide counterparts, namely, the newly developed "P2X" IrO_x/TiO_2 catalyst (HPMG) and the am-IrO_x reference catalyst (Alfa Aesar). The difference in the Ir 4f peak broadening suggests that the crystalline iridium oxides exclusively have a Ir^{4+} surface species, whereas the amorphous oxides possess a mixed iridium oxide character, typical of these types of iridium oxides.[11,32] However, please note that in the latter case, the variety of bond angles and distances that are expected to be present in the amorphous materials arising from their structural disorder could also contribute to the overall peak shape broadening. The analytical fits of the Ir 4f spectra (see Supporting Information, Figure S1) indicate the presence of an additional iridium oxide species ($Ir^{\delta+}$) at a higher binding energy (BE) than the Ir^{4+} species.

The BE of this Ir species is very similar to that of the predicted trivalent Ir-defect sites in a r-IrO_2 atomistic model.[11,32] This indicates that the "P2X" IrO_x/TiO_2 catalyst and the am-IrO_x materials possess a mix of Ir^{4+} and hydroxylated, iridium suboxide species ($Ir^{\delta+}$ where $\delta < 4$). The surface characteristics of the Ir species provide crucial insights into their electrochemical catalytic performance. Previous studies have consistently observed the presence of hydroxylated iridium suboxide species at higher BE than the Ir^{4+} reference under OER relevant conditions, providing the rationale for the enhanced OER activity of amorphous iridium oxides, which exhibit mixed $Ir^{\delta+}/Ir^{4+}$ character, in contrast to their crystalline counterparts.[13,27,33,34] Though the interaction between the metal and the support (metal−support interaction) can affect the electrochemical performance of a catalyst in certain systems,[35,36] our results do not show strong evidence that the underlying TiO_2 structure has altered the

https://doi.org/10.1021/acscatal.4c03562
ACS Catal. 2024, 14, 16759−16769

properties of the electrochemically active iridium oxide (see supporting Ti 2p spectra of the TiO_2 substrates in the Supporting Information).

Differences in the chemical states of the surface iridium oxide species are further evident in the CVs of the catalysts, presented on an equivalent noble metal mass basis (Figure 1b). The CV of the "benchmark" IrO_2/TiO_2 catalyst (in blue) reveals no significant redox features, akin to the r-IrO_2 reference catalyst (in red), confirming the prevalence of the Ir^{4+} surface species in these crystalline catalysts, consistent with previous XPS results. Conversely, the "P2X" IrO_x/TiO_2 catalyst (in green) exhibits strong redox peaks that are similar to the ones that can be observed in the CV of the am-IrO_x reference (in orange), which are characteristic of these amorphous iridium oxides.[15,37] The presence of these redox peaks suggests a material with a flexible iridium chemical nature, often observed in materials containing mixed iridium oxidation states,[17] reaffirming previous XPS results. Am-IrO_x exhibits broader redox peaks and different peak positions compared to the "P2X" IrO_x/TiO_2 catalyst. These differences are likely due to the varying degrees of structural disorder between these materials, which arise from their distinct preparation methods and morphologies. The slightly broader Ir 4f peak (Figure 1a) observed for am-IrO_x, in comparison to the "P2X" IrO_x/TiO_2 catalyst, supports the notion that am-IrOx has a more disordered structure and thus would possess a broader distribution of redox-active sites, leading to the observed variations in peak positions. Consequently, it is anticipated that these two classes of iridium oxides (crystalline and amorphous) undergo different electronic and structural transformations under potential application.

In this study, a mass-based approach is favored for its relevance in cost considerations for PEM water electrolyzers. The absence of a universal metric for assessing electrochemically active surface areas or bulk volumes for iridium-based anode catalysts[38,39] complicates reliable comparisons of reported OER activities, underscoring the need for more standardized protocols.[23,40] To address this challenge and facilitate more meaningful comparisons of commercial-based iridium oxide catalysts, specifically for investigating their structure−property relationships by means of *operando* XAS studies (which also require specific catalyst loadings to obtain high spectral quality[22]), an equivalent noble metal mass basis was adopted in this study.

Electronic Structure of Iridium Oxides under Redox Potentials Probed by Ir L_3-Edge XANES. The electronic structure transformation of the iridium oxides within the redox couple potential regime of 0.3−1.2 V_{RHE} (limiting the upper potential limit to below OER) was probed by means of X-ray absorption near-edge structure (XANES) measurements at the Ir L_3-edge. The leading prominent peaks, known as the white-lines (WLs), of the Ir L_3-edge XANES (Figure 2a) spectra represent dipole-allowed transitions from occupied Ir 2p-derived states to empty Ir 5d-derived states, which are hybridized with O 2p-derived orbitals.[41,42] Despite substantial lifetime broadening (∼5 eV), the WL positions provide crucial insights into the chemical and electronic structure of the probed iridium-containing material. Employing XANES measurements on a metallic iridium reference (Ir^0, having an electron configuration of $5d^7$) and a r-IrO_2 reference (Ir^{4+}, having an electron configuration of $5d^5$), a calibration slope of a 0.92 eV Ir L_3-edge WL shift per formal Ir 5d-band hole count was established (see inset of Figure 2a), aligning with reported literature values ranging between 0.9and 1.3 eV.[43−45] Given the bulk sensitivity of XANES, the average formal iridium oxidation state can therefore be estimated using the established calibration curve (see the inset plot of Figure 2a) and the experimental Ir L_3-edge WL position to infer an average Ir 5*d*-band hole count. Note that this method of interpretation of the Ir L_3-edge WL position assumes a bare surface and does not take into account the influence of any adsorbed species (such as *O, *OH, and *OOH) on the reconfiguration of the Ir 5d unoccupied states probed by XAS.[43]

Utilizing the more conventional stepped CA approach in the range of 0.3−1.2 V_{RHE} (below OER and O_2 generation), *operando* XANES was conducted to study the redox behavior of the "benchmark" IrO_2/TiO_2 catalyst and the "P2X" IrO_x/TiO_2 catalyst, alongside with a comparison to the reference r-IrO_2 and am-IrO_x catalysts (as shown in Figure S5). Both in the anodic and cathodic stepped directions, the crystalline oxides display minimal changes in WL positions, suggesting stable electronic structures under redox potentials (Figure 2b, bottom panel). The average Ir 5d-band hole count, inferred from the experimental Ir L_3-edge WL positions, amounted to 4.7 ± 0.1, corresponding to an average formal oxidation state of $+3.7 \pm 0.1$ for the crystalline iridium oxides within the redox potential range. Thus, these crystalline iridium oxide materials, within acidic electrolyte media, are not purely crystalline Ir^{4+} oxides, however showing a slight reduction in the iridium oxidation state likely due to surface hydration effects at these potentials.[43] Contrarily, the amorphous oxides exhibited substantial, reversible electronic changes within the redox potential region (Figure 2b, bottom panel). The Ir 5d-band hole counts, inferred from the Ir L_3-edge WL positions, range between ∼4 and ∼5, corresponding to formal iridium oxidation states ranging from trivalent Ir-species at lower potentials (>0.3 V_{RHE}) to tetravalent Ir-species at higher potentials (<1.2 V_{RHE}) and reversibly returning to a trivalent Ir-species when stepping down to lower potentials. This showcases the facile and reversible oxidation of amorphous iridium within the potential regime. These trends and the differences in the WL behavior with applied potential aligns well with previous observations on IrO_2 and IrO_x materials.[25,43,46]

The WL position trends of the catalysts demonstrate good alignment with their respective redox couple profiles shown in their CVs (Figure 1b): the crystalline iridium oxides exhibit no prominent redox features, aligning with their stable electronic state, whereas the amorphous iridium oxides exhibit strong redox peaks in line with their substantial and reversible electronic changes as probed via *operando* Ir L_3-edge analysis.

The trends in the iridium oxidation states remain consistent between commercial TiO_2-supported catalysts ("benchmark" IrO_2/TiO_2 catalyst and "P2X" IrO_x/TiO_2 catalyst) and unsupported reference catalysts (r-IrO_2 and am-IrO_x). This alignment is anticipated given the minimal difference in the chemical nature of the iridium species, as evidenced by *ex-situ* XPS measurements (Figure 1a). Therefore, insights derived from the behavior of reference r-IrO_2 and am-IrO_x can effectively contribute to the understanding and interpretation of the performance of supported iridium oxide catalysts.

The "P2X" IrO_x/TiO_2 catalyst exhibits a lower initial iridium oxidation state compared to the "benchmark" IrO_2/TiO_2 catalyst. This divergence, coupled with the distinct trends of the WL positions as a function of applied potential in the redox couple regime, suggests the presence of different active iridium

https://doi.org/10.1021/acscatal.4c03562
ACS Catal. 2024, 14, 16759−16769

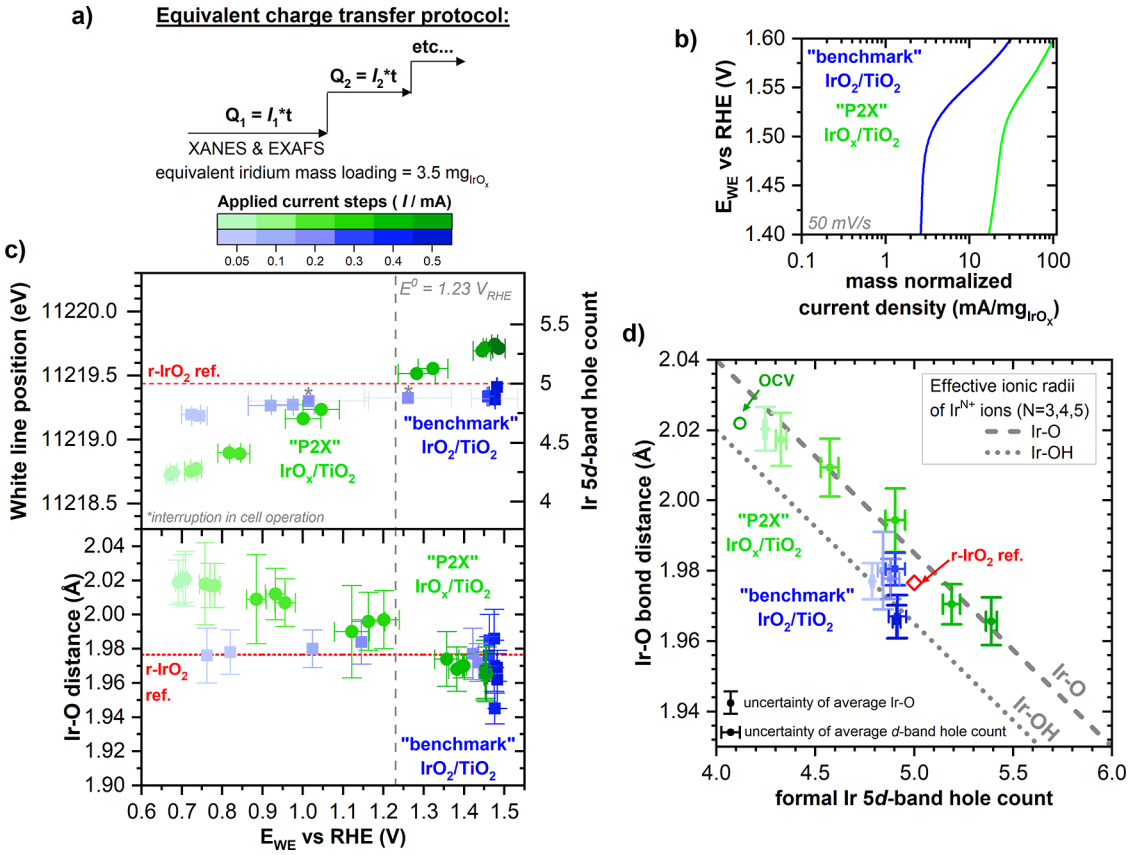

Figure 3. (a) Schematic of the equivalent charge (Q) transfer protocol following chronopotentiometric (CP) steps for the same amount of time ($I \times t$). Color bar legends show the gradient blue and green colors from light to dark corresponding to the stepped current densities from low to high values (0.05−0.60 mA) for the "benchmark" 75 wt %IrO_2/TiO_2 catalyst (in blue) and the "P2X" 30 wt % IrO_x/TiO_2 catalyst (in green). The color legend is also used in subplots (c, d) to indicate the sequential equivalent Q transfer steps. The working electrode loadings were 3.5 mg_{IrOx}. (b) Linear sweep voltammetry from 1.40 to 1.60 V_{RHE} of the "benchmark" and "P2X" electrocatalysts in 0.5 M H_2SO_4 at 50 mV/s. (c) *Operando* Ir L_3-edge XANES WL position (top panel) and EXAFS determined Ir−O bond length (bottom panel) changes upon applying the equivalent Q transfer protocol, with vertical gray dashed lines indicating the theoretical onset potentials for OER at 1.23 V_{RHE}. The horizontal bars in the top and bottom panels represent the range of change of the working electrode potential (E_{we} vs RHE) during collection of the XANES and EXAFS spectra. The WL positions and Ir−O bond lengths are plotted as a function of the median E_{we} value. The horizontal dashed line indicates the WL position of the r-IrO_2 reference. The vertical error bars in the bottom panel represent the error of the Ir−O bond lengths from the EXAFS fitting. The horizontal dashed line indicates the first-shell Ir−O bond length of the r-IrO_2 reference. (d) The average values of the *operando* Ir L_3-edge Ir−O bond distances versus the Ir 5*d*-band hole counts of the "benchmark" 75 wt % IrO_2/TiO_2 catalyst (in blue squares) and the "P2X" 30 wt % IrO_x/TiO_2 catalyst (in green circles). The vertical and horizontal error bars indicate the uncertainties of the average values. The Ir−O bond distance for the dry r-IrO_2 reference is shown by the red square. The dashed and dotted lines represent the theoretical Ir−O and Ir−OH bond distances obtained from ref 47, respectively, determined from the effective ionic radii of Ir^{N+} ions (where N = 3, 4, or 5) and with either O^{I-} or OH^{I-} ions assuming a tetragonal coordination, as reproduced with permission from the International Union of Crystallography.

species and, consequently, different intrinsic activities, likely leading to different OER mechanisms in these commercial catalysts. This fact motivates our exploration of the electronic and structural transformations of these catalysts using our more innovative *operando* spectroscopic-electrochemical protocol, enabling comparative analyses under conditions of equivalent OER activity (i.e., under equivalent O_2 generation and above the range of 0.3−1.2 V_{RHE} measured using the conventional stepped CA approach).

Electronic and Structural Dynamics under Equivalent OER Conditions. *Operando* Ir L_3-edge XANES and extended X-ray absorption fine structure (EXAFS) measurements were performed while employing an equivalent charge transfer (Q) electrochemical protocol following Faraday's law of electrolysis ($Q = I{\cdot}t = n{\cdot}F$). This protocol facilitated a direct comparison of materials with significantly different activities under an equivalent rate of electron transfer (i.e., the same measurable degree of OER), ensuring that the monitored electronic and structural transformations of these commercial materials are evaluated under the same basis of electrocatalytic performance (i.e., the same mass-specific current density (I) for the same time duration (t) and thus the same degree of O_2 production ($n{\cdot}F$)). Figure 3a illustrates the stepped equivalent Q transfer protocol used for the *operando* Ir L_3-edge XANES and EXAFS investigations of the commercial catalysts ("benchmark" IrO_2/TiO_2 catalyst and "P2X" IrO_x/TiO_2 catalyst), with color gradients signifying the stepped mass-specific current densities applied in a low-to-high sequence. The use of this CP-stepped approach is crucial to study these catalysts due to their significantly different electrochemical activities under similar potentials, as depicted in Figure 3b, allowing a well-founded comparison, beyond the CA steps often employed in previous *operando* studies.[25−28]

Figure S6 in the Supporting Information provides a detailed account of the complete time-resolved equivalent Q experiment, encompassing the working electrode voltage (E_{we})

https://doi.org/10.1021/acscatal.4c03562
ACS Catal. 2024, 14, 16759−16769

responses alongside the time durations of the multiple *operando* Ir L_3-edge XANES and EXAFS spectra collected. In Figure 3c, the electronic and local geometric structural transformations of the "benchmark" IrO_2/TiO_2 catalyst (in blue) and the "P2X" IrO_x/TiO_2 catalyst (in green) are depicted as a function of the E_{WE} response, with the horizontal error bars indicating the range of change. The vertical error bars in Figure 3c denote the uncertainty of the Ir−O bond lengths determined from the fitting of the EXAFS spectra. The higher range of the applied CP steps yield E_{WE} responses within the OER region (1.23−1.48 V_{RHE}), making the *operando* measurements directly relevant to PEM-WE operation.

The equivalent *Q* transfer protocol highlights the pronounced electronic structure transformations of the "P2X" IrO_x/TiO_2 catalyst in comparison with the "benchmark" IrO_2/TiO_2 catalyst, particularly under OER-relevant potentials, as evidenced by the large WL position shifts (WL positions in Figure 3c from the Ir L_3-edge XANES spectra shown in Figures S7 and S8). Below OER potentials (<1.2 V_{RHE}), the WL position obtained during the equivalent *Q* transfer protocol are in excellent agreement with those obtained during the stepped CA protocol (Figure S9), affirming the robustness of our approach. At OER conditions (E_{we} = ∼1.48 V_{RHE}), the "P2X" IrO_x/TiO_2 catalyst exhibits an iridium redox state higher than the formal Ir^{4+} state (Ir 5d-band hole count = 5.30 ± 0.02 corresponding to a formal oxidation state of ∼4.3), while the "benchmark" IrO_2/TiO_2 catalyst exhibits a redox state slightly lower than the formal Ir^{4+} state (Ir 5d-band hole count = 4.85 ± 0.03 corresponding to a formal oxidation state of ∼3.9). The evolving Ir−O bond distances, indicative of local geometric structural changes, are presented in Figure 3c (bottom panel), extracted from fittings of k^2-weighted EXAFS spectra obtained during the equivalent *Q* transfer protocol (Figures S10 and S11 and Table S1). At low potentials (low applied current densities), the "P2X" IrO_x/TiO_2 catalyst exhibits a longer first-shell Ir−O bond length compared to the "benchmark" IrO_2/TiO_2 catalyst. This observation aligns with the expected trend, where an increase in the oxidation state of the central iridium ion should lead to a decrease in the Ir−O bond length due to the reduction in its effective ionic radius.[47] Consequently, owing to the higher formal Ir 5*d*-band hole count at low potentials, the "benchmark" IrO_2/TiO_2 catalyst exhibits a shorter Ir−O bond length than the "P2X" IrO_x/TiO_2 catalyst. As the mass-specific current densities are increased (i.e., also increasing E_{we}), both the P2X and "benchmark" catalysts exhibit a reduction in the Ir−O bond lengths, with the P2X catalyst demonstrating a more significant decrease. Particularly under OER relevant conditions of the OER, the P2X catalyst exhibits a further shortening of Ir−O bond lengths with increasing E_{we}, which is in contrast to the "benchmark" catalyst. Toward the upper limits of the measured OER conditions (E_{we} = ∼1.48 V_{RHE}), both materials converge to nearly identical Ir−O bond lengths (∼1.97 Å, see Figure 3c, bottom panel), although the P2X catalyst exhibits a distinctly higher iridium redox state than the "benchmark" catalyst (see Figure 3c, top panel).

This dissimilarity in the electronic and structural behavior of the P2X catalyst and the "benchmark" catalyst can be attributed to variations in their iridium ligand environments. We utilized a combined analysis of the Ir−O bond lengths and Ir 5d hole count information to elucidate the ligand environment surrounding the Ir centers. By plotting Ir−O bond distances against the formal d-band hole count, we can effectively map the changes in the ligand environment, distinguishing between different species such as "Ir−O" and "Ir−OH", which are crucial for catalytic activity. Figure 3d shows the average Ir−O bond lengths obtained from the *operando* EXAFS spectra plotted as a function of the average formal Ir 5d-band hole counts inferred from the average WL positions (Table S2) obtained from the *operando* XANES spectra for each of the mass-specific CP holds in the equivalent *Q* protocol. The dashed reference lines in Figure 3d represent the theoretical Ir−O and Ir−OH ligand configurations, computed from the lengths of effective ionic radii of O^{II-} and OH^{I-} ions with a central Ir^{N+} ion, where *N* = 3, 4, or 5, assuming a tetragonal coordination (Table S3).[47] This approach enables the analysis of the average formal iridium oxidation state and Ir−O bond length obtained from *operando* Ir L_3-edge XANES and EXAFS measurements to infer an "approximate" atomic configuration, between either "Ir−O" or "Ir−OH" type bonds. By implementing an equivalent *Q* transfer protocol and integrating XANES and EXAFS information, our methodology offers an alternative perspective of the different electronic and local geometric structural transformations occurring in these two catalyst materials, enabling detailed property−structure analyses that distinguish between crystalline and amorphous iridium oxide traits.

Figure 3d illustrates the distinct behaviors of the "P2X" IrO_x/TiO_2 catalyst and the "benchmark" IrO_2/TiO_2 catalyst by monitoring their "average" iridium ligand environments. While significant changes in the Ir−O bond lengths and the formal Ir 5d-band hole counts occur (as shown in Figure 3c), the "P2X" IrO_x/TiO_2 catalyst maintains an "average" Ir−O ligand environment with increasing applied mass-specific current densities (i.e., increasing E_{we}). In contrast, the "benchmark" IrO_2/TiO_2 catalyst exhibits a highly stable "average" Ir−OH ligand environment due to the minimal changes in the Ir−O bond lengths and average Ir-oxidation states observed (shown in Figure 3c). These observations under equivalent OER conditions suggest the presence of different atomic configurations in the two different catalyst materials, implying distinct iridium oxide species responsible for their intrinsic activity.

Our adoption of an equivalent *Q* transfer protocol for *operando* Ir L_3-edge XAS, in contrast to the conventional stepped CA hold protocol widely used in previous *operando* XAS and XPS studies,[25−28] ensures a comparative assessment of electronic and structural changes in both the crystalline and amorphous iridium oxide catalysts while they are producing an equivalent amount of O_2.

Previous experiments utilizing the conventional stepped CA hold approach for comparative *operando* studies may have overlooked potential degradation effects due to current densities not being high enough and/or application of equivalent potentials leading to inequivalent amounts of evolving O_2. In scenarios where one catalyst material exhibits significantly lower activity, assertions of "steady-state" or "minimal" electronic and local geometric structure changes under the OER conditions may rather be attributed to the probing of inactive surface areas. Consequently, such analyses could yield skewed property−structure relationships, particularly evident in instances with catalysts with dissimilar electrocatalytic activities. Similarly, when attempting to perform comparisons between existing *operando* XAS studies of different catalyst materials, the large variety of catalyst

https://doi.org/10.1021/acscatal.4c03562
ACS Catal. 2024, 14, 16759−16769

preparation methods and *operando* experimental protocols employed pose a great challenge in achieving a unified analysis of the varying degrees of electronic and structural changes in the different iridium oxides.[21,22] Our approach mitigates potential oversights of degradation effects due to nonuniform electrocatalytic activity and offers more meaningful insights to establish a more accurate, unified evaluation of property−structure relationships in crystalline and amorphous iridium oxides. Furthermore, the unique high surface-to-bulk ratio (due to the nanostructured nature of the catalysts) results in elevated spectroscopic signals pertaining to the active surface species of the OER, offering enhanced clarity in discerning the electronic and structural transformation of the active species in these catalysts while utilizing such a bulk sensitive technique (i.e., XAS).

Our results strongly indicate the presence of distinct mechanisms of the OER in these catalyst materials, attributable to variances in their structural configurations of their active iridium species. The "benchmark" IrO_2/TiO_2 catalyst, characterized by its more stable structure, likely proceeds with an OER mechanism similar to that of r-IrO_2, whereas the highly flexible electronic and structural nature of the "P2X" IrO_x/TiO_2 catalyst points toward an OER mechanism more similar to am-IrO*x*,[17] given the similarity in their behaviors. The decrease in the Ir−O bond length in the "P2X" catalyst under OER relevant conditions, which "benchmark" catalyst does not exhibit, suggests the formation of active sites with higher intrinsic activity.[43] Here, we provided insights into the formation of dangling O bonds and edge termination bonds at defect sites under OER conditions, which exhibit significantly shorter Ir−O bond lengths compared to the pristine lattice structure. Formation of these defect sites is responsible for the formation of highly active sites with significantly lower activation energy barriers for the OER. Thus, the reduction in the average Ir−O bond length serves as a compelling indicator of the formation of these active sites that originate from defect sites within the material. Analogous to the effect observed in highly active, defective iridium oxide catalysts, our evidence of significant contraction of the Ir−O bond lengths of the "P2X" catalyst under OER relevant conditions lends support to our understanding of why the "P2X" IrO_x/TiO_2 catalyst outperforms the "benchmark" IrO_2/TiO_2 catalyst, as evidenced by significantly higher mass-specific activity of the former during a long-term PEM water electrolyzer performance test.[9,10] The increased intrinsic activity of the "P2X" catalyst, due to formation of these defect sites as evidenced by the strong change in the Ir−O bond lengths inferring multiple active sites, contributes to its significantly superior performance, despite its lower intrinsic conductivity compared to that of the "benchmark" catalyst.[9,10] Furthermore, the difference in the "average" atomic configuration of the crystalline and amorphous commercial catalysts, as shown in Figure 3d, indirectly highlights different mechanisms influencing the stability of the iridium species in each of the catalysts. Addressing the difference in the long-term performances of the "P2X" IrO_x/TiO_2 catalyst and the "benchmark" IrO_2/TiO_2 catalyst as shown in ref 10, the results of our study hint toward the need for different approaches to increase the relative stability and performance of the "P2X" IrO_x/TiO_2 catalyst, given its unique electronic configuration. Tailored strategies such as moderate thermal treatment of TiO_2-supported amorphous iridium oxides, resulting in semicrystalline IrO_x formation, emerges as a promising avenue.[7] Given the delicate balance of high activity−conductivity−stability required of commercially viable iridium oxide-based anode catalyst materials, the "P2X" IrO_x/TiO_2 catalyst demonstrates a structure−property relationship that gives confidence in the promise of its large-scale commercial use.

Our developed equivalent *Q* transfer protocol consistently provides accurate electronic and structural insights for potentials below OER (<1.23 V_{RHE}), aligning well with data obtained via the conventional stepped CA approach, thus validating our method's reliability. Moreover, our developed protocol enables meaningful comparisons of the electronic and structural transformations under equivalent OER conditions (1.23−1.48 V_{RHE}) across iridium oxide-based catalysts with varying activities, a task less straightforward with the stepped CA approach, by adopting techniques akin to conventional electrochemical catalyst comparisons.[23,24] Our approach enables a cohesive and unified spectroscopic-electrochemical assessment of different iridium oxide-based catalysts.

We propose for the adoption of *operando* Ir L_3-edge XANES and EXAFS employing equivalent *Q* transfer protocols as an effective technique unravelling property−structure relationships between different types of iridium oxide-based catalysts under OER conditions and as a useful technique to evaluate industrially synthesized iridium oxide catalysts. This approach provided crucial insights into the intricate electronic and structural dynamics of the "P2X" IrO_x/TiO_2 catalyst and its comparison to the current commercial "benchmark" IrO_2/TiO_2 catalyst under equivalent, relevant OER conditions. The discernible differences in the iridium ligand environments and corresponding OER mechanisms between the crystalline and amorphous catalysts underscore the necessity for different tailored strategies to enhance their long-term performance in real-world applications, thereby advancing our understanding in the field of PEM-WE.

CONCLUSIONS

Our investigation using *operando* Ir L_3-edge XAS has provided crucial insights into the behavior of industrially synthesized iridium oxide catalysts under OER relevant conditions, thereby also facilitating a direct comparison between two different classes of iridium oxides. The "P2X" IrO_x/TiO_2 catalyst exhibits a potential-dependent variation of the iridium oxidation state analogous to a reference amorphous iridium oxide, whereas the "benchmark" IrO_2/TiO_2 catalyst displays minimal oxidation state changes, comparable to r-IrO_2. These spectroscopic trends mirror the distinct electrochemical redox behaviors of the crystalline and amorphous iridium oxide-based catalysts, emerging as indirect descriptors of their PEM-WE performance.

To enable the correlation of the chemical structural transformations of the catalysts with their distinct electrochemical performances, an innovative *operando* spectroscopic-electrochemical protocol was applied in this study. Based on a conventional lab-based electrochemical activity benchmarking procedure, equivalent OER conditions in different catalysts (i.e., resulting in a similar O_2 production) are ensured by an equivalent charge transfer approach. This systematic evaluation of their structure−property relationships by *operando* Ir L_3-edge XAS enables meaningful comparisons between catalysts with very distinct electrochemical responses, such as the two catalysts compared in this study. Under this newly developed standardized spectroscopic-electrochemical protocol, the "P2X" IrO_x/TiO_2 catalyst displays large shifts in the WL

https://doi.org/10.1021/acscatal.4c03562
ACS Catal. 2024, 14, 16759−16769

position derived from the *operando* Ir L_3-edge XANES spectra indicating a flexible oxidation nature, whereas the "benchmark" IrO_2/TiO_2 catalyst possesses a more stable oxidation state. Correlated with the large shifts in the WL position at OER relevant conditions, the "P2X" IrO_x/TiO_2 catalyst displays strong contractions of the average Ir−O bond lengths derived from *operando* EXAFS.

In conclusion, the *operando* Ir L_3-edge XANES and EXAFS results reveal that the two studied catalysts possess different "average" atomic configurations. By virtue of the equivalent charge transfer protocol used in this study, the atomistic insights can be linked to the distinct PEM-WE performances of these catalysts, bridging the gap between fundamental knowledge and industrial application. Furthermore, the observed differences in the "average" iridium ligand environments, and its consequent implication on the different OER mechanisms, indicate the need for individual, tailored strategies for stabilizing their long-term performance in practical applications.

MATERIALS AND METHODS

Iridium Oxide Catalysts. The current commercial benchmark iridium-based OER catalyst, 75 wt % IrO_2/TiO_2 Umicore Elyst 0480, and the newly designed OER anode catalyst within the framework of the Kopernikus P2X project,[8] 30 wt % IrO_x/TiO_2, are studied in this work. The two commercial catalysts were studied as-received without any treatment. For comparison, two additional reference iridium oxide powders were also studied: r-IrO_2 (Sigma-Aldrich) and amorphous (hydrous) iridium oxide (Alfa Aesar) referred to as am-IrO_x. am-IrO_x has been previously characterized by Pfeifer et al.[11,27,32] The r-IrO_2 catalyst was first annealed at 600 °C for 2 h to form the highly crystalline version. This forms a comparison basis of both crystalline and amorphous catalysts and unsupported and TiO_2-supported catalysts in order to elucidate the behavior of the commercially available OER catalysts. Table 1 summarizes the catalysts used within this study.

Table 1. Iridium Oxide Catalysts

catalysts	supplier
r-IrO_2[a]	Sigma-Aldrich (99.9% trace metals basis)
am-IrO_x	Alfa Aesar, Premion, 99.99% trace metals basis
75 wt.% IrO_2/TiO_2	Umicore Elyst Ir75 0480
30 wt.% IrO_x/TiO_2	Heraeus Precious Metals GmbH & Co. KG, Germany

[a]Thermally pretreated at 600 °C for 2 h in air.

***Ex Situ* XPS.** *Ex situ* XPS measurements of the catalyst powders were performed using a nonmonochromatized Al K_α excitation X-ray source (1486.6 eV, PREVAC RS40B1) and a ScientaOmicron Argus CU analyzer attached to the off-synchrotron analysis chamber located in the Energy Materials In Situ Laboratory Berlin (EMIL). The samples were mounted using carbon-tape and measured using a pass energy of 20 eV for core-level spectra and 100 eV for survey spectra. The chamber pressure was kept to $<5 \times 10^{-8}$ mbar during measurements. The XPS core-level spectra were fitted using the LMFIT Python package[48] (see Figure S1). The line shape parameters of the Ir^{4+} species were determined by fits of the IrO_2 reference XPS data.

Electrode Preparations. Catalyst ink solutions were prepared from catalyst powders, isopropanol (purity ≥99.9%, Sigma-Aldrich), Nafion ionomer solution (5 wt %, ionomer, LIQUion solution LQ-1005), and ultrapure water (Millipore, 18 Ω), such that a solution density of 270 $mg_{catalyst}$/mL and a 10 wt % ionomer content was obtained, with a 1:1 ratio of isopropanol and water. The catalyst ink solution was sonicated in an ultrasonic bath for 30 min prior to drop-casting. For both *ex situ* electrochemical and *operando* Ir L_3-edge XAS measurements, certain volumes of catalyst ink were pipetted onto a precleaned 300 μm thick glassy carbon plate (SigradurG) to achieve a final loading of 3.5 mg_{IrOx}/cm^2 for each catalyst powder and dried for 2 h in air to form a thin uniform catalyst film.

Electrochemical Characterizations. *Ex situ* electrochemical measurements were performed using a BioLogic SP-300 potentiostat in a beaker with 0.5 M H_2SO_4 electrolyte solutions and a Pt mesh (52 mesh woven, 0.1 mm diameter wire, 99.9% Alfa Aesar) as the counter electrode (CE) and a reversible hydrogen electrode (Mini HydroFlex, Gaskatel) as the reference electrode (RE). The catalysts were conditioned by cycling between 0.05 and 1.4 V_{RHE} at 50 mV/s for 50 cycles until steady-state CVs of the material were achieved for electrochemical characterization. Figure 1 shows the 50th cycle of each of the catalyst powders, and Figure S2 shows the evolution of the CVs upon conditioning.

***Operando* Ir L_3-Edge XAS.** The iridium oxide catalysts were evaluated with *operando* XAS measurements in transmission-mode (see Figure S3 for the experimental setup) using an in-house designed electrochemical transmission cell (see Figure S4 for the cell design). The samples were prepared by drop-casting certain volumes of catalyst ink solutions, as described above, to achieve mass equivalent loadings of iridium (3.5 mg_{IrOx}) onto glassy carbon plates (300 μm thick, SigradurG). The electrodes were prewetted prior to assembly in the electrochemical cell by covering them with a droplet of ultrapure water. This reduced the amount of trapped bubbles within the catalyst layer once the electrolyte was filled into the electrochemical cell. The glassy carbon plates acted both as WE and as the X-ray transparent window in the cell. The exposed area of the WE to the electrolyte solution (also the circular transmission window size) was 113 mm^2 (radii = 6 mm). The same CE and RE, H_2SO_4 electrolyte concentration, and potentiostat as mentioned before were used for these experiments, and the same initial conditioning process was also carried out in the electrochemical transmission cell prior to XAS acquisition. Electrochemical impedance spectroscopy was carried out for *iR* correction of the *operando* XAS protocols.

The *operando* Ir L_3-edge XANES and EXAFS measurements were performed at the High Resolution Powder Diffraction (HRPD)-XAS endstation at the NOTOS beamline from the ALBA Synchrotron Light Source, located in Cerdanyola del Vallès, near Barcelona (Spain). Synchrotron light from a bending magnet was first vertically collimated, then monochromatized using two pairs of water-cooled Si(111) crystals, and finally focused to the sample position down to ∼500 × 500 μm^2. The beamline is equipped with three ion chambers for transmission mode XAS measurements and a 13-element energy-resolving silicon drift detector at 45° with respect to the incoming X-rays for fluorescence mode XAS measurements. The XAS measurements were performed in transmission mode, with the reference standard (compact r-IrO_2 powder thin pellet) after behind the electrochemical cell and between the second and third ionization chambers, for checking the energy calibration. The XANES and EXAFS spectra were

https://doi.org/10.1021/acscatal.4c03562
ACS Catal. 2024, 14, 16759−16769

collected using 0.2 and 0.9 eV step sizes, respectively. The electrochemical transmission cell was mounted on a motorized xyz sample stage for sample alignment.

Operando Ir L_3-edge XAS spectra were first collected by stepped chronoamperometry (CA) applications in the range of 0.3−1.2 V_{RHE} in both the anodic and cathodic directions to study the redox behavior for each iridium catalyst. During each potentiostatic hold, several XANES and EXAFS measurements were taken and averaged to achieve adequate spectral quality.

The behavior of the catalysts under relevant conditions under the OER was studied using an equivalent charge (Q) transfer protocol (Figure S6). Freshly prepared and conditioned electrodes were used for these experiments. Chronopotentiometry (CP) holds at 0.05, 0.1, 0.2, 0.3, 0.4, 0.5, and 0.6 mA for 30 min each were carried out for each catalyst. This resulted in equivalent charge transfer (mA/mg_{Ir}) for each catalyst (given their equivalent IrO_x mass loadings) according to Faraday's law of electrolysis ($Q = I{\cdot}t = n{\cdot}F$), where I is the applied current, t is the time, n is the number of moles of O_2 evolved, and F is Faraday's constant. This allows for an equivalent activity (i.e., number of moles of O_2 evolved) experiment for catalysts with different iridium loadings [i.e., "P2X" IrO_x/TiO_2 (30 wt %) catalyst versus the "benchmark" IrO_2/TiO_2 (75 wt %) catalyst] while monitoring their electronic and local geometric structural changes by XAS. While the currents employed in these experiments are lower than those used in the PEM-WE stability measurements of these materials,[9,10] the E_{WE} potentials achieved during these holds (∼1.48 V_{RHE}) are well within the OER region, ensuring that the catalytic processes studied by *operando* XAS are directly relevant to PEM-WE operation. During the 30 min hold, two XANES and four EXAFS measurements were taken. For each XAS measurement (under potential or CP hold), the catalyst was given some time (∼2 min) to stabilize before the XAS measurements were taken.

The XANES and EXAFS raw data were processed (deglitched, averaged where applicable, and normalized) using the ATHENA program,[49] and EXAFS refinements were performed using Larch software package.[50] The energy position of the WL was determined by the minimum of the second derivative.[51,52] The EXAFS refinements were performed for the k^2-weighted spectra over the region k = 3−11 $Å^{-1}$ and R = 1−2.5 Å (Figures S10 and S11). The ab initio atomic scattering paths were constructed using the FEFF 8.0 code interfaced within the Larch package. The passive electron reduction factor (S_0^2) was determined from refinements of the dry IrO_2 powder and used in the EXAFS fittings of all other catalyst materials. EXAFS refinements were performed for the first shell Ir−O scattering path using a tetragonal IrO_2 model, with relaxed interatomic distances and coordination numbers.

■ ASSOCIATED CONTENT

Data Availability Statement

The data that support the findings of this study is available on a Zenodo online repository and has the following permanent DOI: https://zenodo.org/doi/10.5281/zenodo.11383412

Supporting Information

The Supporting Information is available free of charge at https://pubs.acs.org/doi/10.1021/acscatal.4c03562.

Additional information regarding the analytical fittings for Ir 4f core-level spectra; electrochemical characterization; experimental configuration for *operando* Ir L3-edge XAS measurements; the electrochemical transmission cell used; the *operando* XANES and EXAFS spectra collected during stepped potential application and during the equivalent charge transfer protocol; and the EXAFS fit results (PDF)

■ AUTHOR INFORMATION

Corresponding Authors

Marianne van der Merwe − *Department Interface Design, Helmholtz-Zentrum Berlin Für Materialien und Energie GmbH (HZB), Berlin 12489, Germany;* orcid.org/0000-0002-3182-1392; Email: marianne.vdm@helmholtz-berlin.de

Raul Garcia-Diez − *Department Interface Design, Helmholtz-Zentrum Berlin Für Materialien und Energie GmbH (HZB), Berlin 12489, Germany;* orcid.org/0009-0000-9374-1083; Email: raul.garcia_diez@helmholtz-berlin.de

Authors

Romualdus Enggar Wibowo − *Department Interface Design, Helmholtz-Zentrum Berlin Für Materialien und Energie GmbH (HZB), Berlin 12489, Germany;* orcid.org/0000-0002-8325-0413

Catalina E. Jimenez − *Department Interface Design, Helmholtz-Zentrum Berlin Für Materialien und Energie GmbH (HZB), Berlin 12489, Germany;* orcid.org/0000-0002-8107-4399

Carlos Escudero − *ALBA Synchrotron Light Source, Barcelona 08290, Spain;* orcid.org/0000-0001-8716-9391

Giovanni Agostini − *ALBA Synchrotron Light Source, Barcelona 08290, Spain;* Present Address: ELETTRA Sincrotrone Trieste S.C.p.A., S.S. 14 Km 163.5, 34149 Trieste, Italy

Marcus Bär − *Department Interface Design, Helmholtz-Zentrum Berlin Für Materialien und Energie GmbH (HZB), Berlin 12489, Germany; Energy Materials In-situ Laboratory Berlin (EMIL), HZB, Berlin 12489, Germany; Department of Chemistry and Pharmacy, Friedrich-Alexander-Universität Erlangen-Nürnberg, Erlangen 91058, Germany; Department of X-ray Spectroscopy at Interfaces of Thin Films, Helmholtz Institute Erlangen-Nürnberg for Renewable Energy (HI ERN), Berlin 12489, Germany;* orcid.org/0000-0001-8581-0691

Complete contact information is available at: https://pubs.acs.org/10.1021/acscatal.4c03562

Author Contributions

Conceptualization and project administration: M.vdM. and R.G.D. Data curation of XAS: M.vdM., R.E.W., C.E.J., and R.G.D. conducted the XAS experiments with the support of C.E. and G.A. Data curation of electrochemical characterization and XPS measurements: M.vdM. Data analysis: M.vdM. Funding acquisition: M.B. Writing−original manuscript and figures: M.vdM. Writing−review and editing: R.E.W., C.E.J., C.E., G.A., M.B., and R.G.D. All authors have given approval to the final version of the manuscript.

Notes

The authors declare no competing financial interest.

https://doi.org/10.1021/acscatal.4c03562
ACS Catal. 2024, 14, 16759−16769

■ ACKNOWLEDGMENTS

This work was funded by the German Federal Ministry of Education and Research (BMBF) within the framework of the Kopernikus P2X project (03SFK2 × 0) (HZB). M.vdM. acknowledges the support from the Graduate School Materials for Solar Energy Conversion (MatSEC) as part of the Dahlem Research School. R.G.-D. acknowledges support from BMBF in the framework of the project CatLab, Germany (03EW0015A/B). We thank Prof. H.A. Gasteiger, the chair of Technical Electrochemistry at the Technical University of Munich, for organization of the Kopernikus P2X work-package. The authors would also like to thank Maximillian Möckl from the ZAE Bayern for provision of the Umicore commercial benchmark catalyst, Chistian Gebauer from Heraeus Precious Metals GmbH & Co. KG for provision of the "P2X" catalyst, and Axel Knop-Gericke from Fritz-Haber Institut (FHI, Berlin) for provision of the am-IrO_x reference catalyst. The authors also thank ALBA for allocation of synchrotron radiation beamtime under the proposal no. 2021095412 at NOTOS. The Energy Materials In-Situ Laboratory Berlin (EMIL) is acknowledged for providing the infrastructure to allow for off-synchrotron, lab-source X-ray analytic measurements.

■ REFERENCES

(1) Schlögl, R. The Role of Chemistry in the Energy Challenge. *ChemSusChem* **2010**, *3* (2), 209−222.
(2) Bernt, M.; Hartig-Weiß, A.; Tovini, M. F.; El-Sayed, H. A.; Schramm, C.; Schröter, J.; Gebauer, C.; Gasteiger, H. A. Current Challenges in Catalyst Development for PEM Water Electrolyzers. *Chem. Ing. Tech.* **2020**, *92* (1−2), 31−39.
(3) Fabbri, E.; Habereder, A.; Waltar, K.; Kötz, R.; Schmidt, T. J. Developments and Perspectives of Oxide-Based Catalysts for the Oxygen Evolution Reaction. *Catal. Sci. Technol.* **2014**, *4* (11), 3800−3821.
(4) Bernt, M.; Siebel, A.; Gasteiger, H. A. Analysis of Voltage Losses in PEM Water Electrolyzers with Low Platinum Group Metal Loadings. *J. Electrochem. Soc.* **2018**, *165* (5), F305−F314.
(5) Hartig-Weiss, A.; Miller, M.; Beyer, H.; Schmitt, A.; Siebel, A.; Freiberg, A. T. S.; Gasteiger, H. A.; El-Sayed, H. A. Iridium Oxide Catalyst Supported on Antimony-Doped Tin Oxide for High Oxygen Evolution Reaction Activity in Acidic Media. *ACS Appl. Nano Mater.* **2020**, *3* (3), 2185−2196.
(6) Rajan, Z. S. H. S.; Binninger, T.; Kooyman, P. J.; Susac, D.; Mohamed, R. Organometallic Chemical Deposition of Crystalline Iridium Oxide Nanoparticles on Antimony-Doped Tin Oxide Support with High-Performance for the Oxygen Evolution Reaction. *Catal. Sci. Technol.* **2020**, *10* (12), 3938−3948.
(7) Böhm, D.; Beetz, M.; Gebauer, C.; Bernt, M.; Schröter, J.; Kornherr, M.; Zoller, F.; Bein, T.; Fattakhova-Rohlfing, D. Highly Conductive Titania Supported Iridium Oxide Nanoparticles with Low Overall Iridium Density as OER Catalyst for Large-Scale PEM Electrolysis. *Appl. Mater. Today* **2021**, *24*, 101134.
(8) Kopernikus P2X project funded by the German Ministry of Education and Research (BMBF). https://www.kopernikus-projekte.de/en/projects/p2x (accessed November 09, 2023).
(9) Bernt, M.; Schramm, C.; Schröter, J.; Gebauer, C.; Byrknes, J.; Eickes, C.; Gasteiger, H. A. Effect of the IrO_x Conductivity on the Anode Electrode/Porous Transport Layer Interfacial Resistance in PEM Water Electrolyzers. *J. Electrochem. Soc.* **2021**, *168* (8), 084513.
(10) Möckl, M.; Ernst, M. F.; Kornherr, M.; Allebrod, F.; Bernt, M.; Byrknes, J.; Eickes, C.; Gebauer, C.; Moskovtseva, A.; Gasteiger, H. A. Durability Testing of Low-Iridium PEM Water Electrolysis Membrane Electrode Assemblies. *J. Electrochem. Soc.* **2022**, *169* (6), 064505.
(11) Pfeifer, V.; Jones, T. E.; Velasco Vélez, J. J.; Massué, C.; Greiner, M. T.; Arrigo, R.; Teschner, D.; Girgsdies, F.; Scherzer, M.; Allan, J.; Hashagen, M.; Weinberg, G.; Piccinin, S.; Hävecker, M.; Knop-Gericke, A.; Schlögl, R. The Electronic Structure of Iridium Oxide Electrodes Active in Water Splitting. *Phys. Chem. Chem. Phys.* **2016**, *18* (4), 2292−2296.
(12) Schweinar, K.; Gault, B.; Mouton, I.; Kasian, O. Lattice Oxygen Exchange in Rutile IrO_2 during the Oxygen Evolution Reaction. *J. Phys. Chem. Lett.* **2020**, *11* (13), 5008−5014.
(13) Velasco-Vélez, J. J.; Carbonio, E. A.; Chuang, C.-H.; Hsu, C.-J.; Lee, J.-F.; Arrigo, R.; Hävecker, M.; Wang, R.; Plodinec, M.; Wang, F. R.; Centeno, A.; Zurutuza, A.; Falling, L. J.; Mom, R. V.; Hofmann, S.; Schlögl, R.; Knop-Gericke, A.; Jones, T. E. Surface Electron-Hole Rich Species Active in the Electrocatalytic Water Oxidation. *J. Am. Chem. Soc.* **2021**, *143* (32), 12524−12534.
(14) Velasco-Vélez, J.; Jones, T. E.; Streibel, V.; Hävecker, M.; Chuang, C. H.; Frevel, L.; Plodinec, M.; Centeno, A.; Zurutuza, A.; Wang, R.; Arrigo, R.; Mom, R.; Hofmann, S.; Schlögl, R.; Knop-Gericke, A. Electrochemically Active Ir NPs on Graphene for OER in Acidic Aqueous Electrolyte Investigated by in Situ and Ex Situ Spectroscopies. *Surf. Sci.* **2019**, *681*, 1−8.
(15) Cherevko, S.; Geiger, S.; Kasian, O.; Mingers, A.; Mayrhofer, K. J. J. Oxygen Evolution Activity and Stability of Iridium in Acidic Media. Part 2. - Electrochemically Grown Hydrous Iridium Oxide. *J. Electroanal. Chem.* **2016**, *774*, 102−110.
(16) Saveleva, V. A.; Wang, L.; Teschner, D.; Jones, T.; Gago, A. S.; Friedrich, K. A.; Zafeiratos, S.; Schlögl, R.; Savinova, E. R. Operando Evidence for a Universal Oxygen Evolution Mechanism on Thermal and Electrochemical Iridium Oxides. *J. Phys. Chem. Lett.* **2018**, *9* (11), 3154−3160.
(17) Geiger, S.; Kasian, O.; Ledendecker, M.; Pizzutilo, E.; Mingers, A. M.; Fu, W. T.; Diaz-Morales, O.; Li, Z.; Oellers, T.; Fruchter, L.; Ludwig, A.; Mayrhofer, K. J. J.; Koper, M. T. M.; Cherevko, S. The Stability Number as a Metric for Electrocatalyst Stability Benchmarking. *Nat. Catal.* **2018**, *1* (7), 508−515.
(18) Kasian, O.; Geiger, S.; Li, T.; Grote, J. P.; Schweinar, K.; Zhang, S.; Scheu, C.; Raabe, D.; Cherevko, S.; Gault, B.; Mayrhofer, K. J. J. Degradation of Iridium Oxides via Oxygen Evolution from the Lattice: Correlating Atomic Scale Structure with Reaction Mechanisms. *Energy Environ. Sci.* **2019**, *12* (12), 3548−3555.
(19) Diklić, N.; Clark, A. H.; Herranz, J.; Aegerter, D.; Diercks, J. S.; Beard, A.; Saveleva, V. A.; Chauhan, P.; Nachtegaal, M.; Huthwelker, T.; Lebedev, D.; Kayser, P.; Alonso, J. A.; Copéret, C.; Schmidt, T. J. Surface Ir+5 Formation as a Universal Prerequisite for O_2 Evolution. *ACS Catal.* **2023**, *13* (16), 11069−11079.
(20) Velasco Vélez, J. J.; Bernsmeier, D.; Mom, R. V.; Zeller, P.; Shao-Horn, Y.; Roldan Cuenya, B.; Knop-Gericke, A.; Schlögl, R.; Jones, T. E. Iridium Oxide Coordinatively Unsaturated Active Sites Govern the Electrocatalytic Oxidation of Water. *Adv. Energy Mater.* **2024**, *14* (19), 2303407.
(21) Naito, T.; Shinagawa, T.; Nishimoto, T.; Takanabe, K. Recent Advances in Understanding Oxygen Evolution Reaction Mechanisms over Iridium Oxide. *Inorg. Chem. Front.* **2021**, *8* (11), 2900−2917.
(22) Diklić, N.; Clark, A. H.; Herranz, J.; Diercks, J. S.; Aegerter, D.; Nachtegaal, M.; Beard, A.; Schmidt, T. J. Potential Pitfalls in the Operando XAS Study of Oxygen Evolution Electrocatalysts. *ACS Energy Lett.* **2022**, *7* (5), 1735−1740.
(23) Risch, M. Reporting Activities for the Oxygen Evolution Reaction. *Commun. Chem.* **2023**, *6* (1), 221−225.
(24) Zlatar, M.; Escalera-López, D.; Rodríguez, M. G.; Hrbek, T.; Götz, C.; Mary Joy, R.; Savan, A.; Tran, H. P.; Nong, H. N.; Pobedinskas, P.; Briega-Martos, V.; Hutzler, A.; Böhm, T.; Haenen, K.; Ludwig, A.; Khalakhan, I.; Strasser, P.; Cherevko, S. Standardizing OER Electrocatalyst Benchmarking in Aqueous Electrolytes: Comprehensive Guidelines for Accelerated Stress Tests and Backing Electrodes. *ACS Catal.* **2023**, *13* (23), 15375−15392.
(25) Ruiz Esquius, J.; Morgan, D. J.; Algara Siller, G.; Gianolio, D.; Aramini, M.; Lahn, L.; Kasian, O.; Kondrat, S. A.; Schlögl, R.; Hutchings, G. J.; Arrigo, R.; Freakley, S. J. Lithium-Directed

https://doi.org/10.1021/acscatal.4c03562
ACS Catal. 2024, 14, 16759−16769

Transformation of Amorphous Iridium (Oxy)Hydroxides To Produce Active Water Oxidation Catalysts. *J. Am. Chem. Soc.* **2023**, *145* (11), 6398−6409.
(26) Minguzzi, A.; Lugaresi, O.; Achilli, E.; Locatelli, C.; Vertova, A.; Ghigna, P.; Rondinini, S. Observing the Oxidation State Turnover in Heterogeneous Iridium-Based Water Oxidation Catalysts. *Chem. Sci.* **2014**, *5* (9), 3591−3597.
(27) Pfeifer, V.; Jones, T. E.; Velasco Vélez, J. J.; Arrigo, R.; Piccinin, S.; Hävecker, M.; Knop-Gericke, A.; Schlögl, R. In Situ Observation of Reactive Oxygen Species Forming on Oxygen-Evolving Iridium Surfaces. *Chem. Sci.* **2017**, *8* (3), 2143−2149.
(28) Saveleva, V. A.; Wang, L.; Luo, W.; Zafeiratos, S.; Ulhaq-Bouillet, C.; Gago, A. S.; Friedrich, K. A.; Savinova, E. R. Uncovering the Stabilization Mechanism in Bimetallic Ruthenium-Iridium Anodes for Proton Exchange Membrane Electrolyzers. *J. Phys. Chem. Lett.* **2016**, *7* (16), 3240−3245.
(29) McCrory, C. C. L.; Jung, S.; Peters, J. C.; Jaramillo, T. F. Benchmarking Heterogeneous Electrocatalysts for the Oxygen Evolution Reaction. *J. Am. Chem. Soc.* **2013**, *135* (45), 16977−16987.
(30) McCrory, C. C. L.; Jung, S.; Ferrer, I. M.; Chatman, S. M.; Peters, J. C.; Jaramillo, T. F. Benchmarking Hydrogen Evolving Reaction and Oxygen Evolving Reaction Electrocatalysts for Solar Water Splitting Devices. *J. Am. Chem. Soc.* **2015**, *137* (13), 4347−4357.
(31) Werner, W. S. M.; Smekal, W.; Powell, C. J. *Simulation of Electron Spectra for Surface Analysis (SESSA) - Version 2.1*; National Institute of Standards and Technology: Gaithersburg, MD, 2016.
(32) Pfeifer, V.; Jones, T. E.; Velasco Vélez, J. J.; Massué, C.; Arrigo, R.; Teschner, D.; Girgsdies, F.; Scherzer, M.; Greiner, M. T.; Allan, J.; Hashagen, M.; Weinberg, G.; Piccinin, S.; Hävecker, M.; Knop-Gericke, A.; Schlögl, R. The Electronic Structure of Iridium and Its Oxides. *Surf. Interface Anal.* **2016**, *48* (5), 261−273.
(33) Frevel, L. J.; Mom, R.; Velasco-Vélez, J. J.; Plodinec, M.; Knop-Gericke, A.; Schlögl, R.; Jones, T. E. In Situ X-Ray Spectroscopy of the Electrochemical Development of Iridium Nanoparticles in Confined Electrolyte. *J. Phys. Chem. C* **2019**, *123* (14), 9146−9152.
(34) Casalongue, H. S.; Kaya, S.; Viswanathan, V.; Miller, D. J.; Friebel, D.; Hansen, H. A.; Nørskov, J. K.; Nilsson, A.; Ogasawara, H. Direct Observation of the Oxygenated Species during Oxygen Reduction on a Platinum Fuel Cell Cathode. *Nat. Commun.* **2013**, *4* (1), 2817.
(35) Luo, Z.; Zhao, G.; Pan, H.; Sun, W. Strong Metal − Support Interaction in Heterogeneous. *Catalysts* **2022**, *2201395*, 1−15.
(36) Moriau, L.; Smiljanić, M.; Lončar, A.; Hodnik, N. Supported Iridium-Based Oxygen Evolution Reaction Electrocatalysts - Recent Developments. *ChemCatChem* **2022**, *14* (20), 202200586.
(37) Geiger, S.; Kasian, O.; Shrestha, B. R.; Mingers, A. M.; Mayrhofer, K. J. J.; Cherevko, S. Activity and Stability of Electrochemically and Thermally Treated Iridium for the Oxygen Evolution Reaction. *J. Electrochem. Soc.* **2016**, *163* (11), F3132−F3138.
(38) Alia, S. M.; Hurst, K. E.; Kocha, S. S.; Pivovar, B. S. Mercury Underpotential Deposition to Determine Iridium and Iridium Oxide Electrochemical Surface Areas. *J. Electrochem. Soc.* **2016**, *163* (11), F3051−F3056.
(39) Tan, X.; Shen, J.; Semagina, N.; Secanell, M. Decoupling Structure-Sensitive Deactivation Mechanisms of Ir/IrOx Electrocatalysts toward Oxygen Evolution Reaction. *J. Catal.* **2019**, *371*, 57−70.
(40) Bligaard, T.; Bullock, R. M.; Campbell, C. T.; Chen, J. G.; Gates, B. C.; Gorte, R. J.; Jones, C. W.; Jones, W. D.; Kitchin, J. R.; Scott, S. L. Toward Benchmarking in Catalysis Science: Best Practices, Challenges, and Opportunities. *ACS Catal.* **2016**, *6* (4), 2590−2602.
(41) Clancy, J. P.; Chen, N.; Kim, C. Y.; Chen, W. F.; Plumb, K. W.; Jeon, B. C.; Noh, T. W.; Kim, Y.-J. Spin-Orbit Coupling in Iridium-Based 5d Compounds Probed by x-Ray Absorption Spectroscopy. *Phys. Rev. B* **2012**, *86* (19), 195131.
(42) Choy, J.-H.; Kim, D.-K.; Demazeau, G.; Jung, D.-Y. L_{III}-Edge XANES Study on Unusually High Valent Iridium in a Perovskite Lattice. *J. Phys. Chem.* **1994**, *98* (25), 6258−6262.
(43) Nong, H. N.; Reier, T.; Oh, H. S.; Gliech, M.; Paciok, P.; Vu, T. H. T.; Teschner, D.; Heggen, M.; Petkov, V.; Schlögl, R.; Jones, T.; Strasser, P. A Unique Oxygen Ligand Environment Facilitates Water Oxidation in Hole-Doped $IrNiO_x$ Core−Shell Electrocatalysts. *Nat. Catal.* **2018**, *1* (11), 841−851.
(44) Mo, Y.; Stefan, I. C.; CaiDongCareyScherson, W. J. P. D. A.; Dong, J.; Carey, P.; Scherson, D. A. In Situ Iridium L_{III}-Edge X-Ray Absorption and Surface Enhanced Raman Spectroscopy of Electrodeposited Iridium Oxide Films in Aqueous Electrolytes. *J. Phys. Chem. B* **2002**, *106* (14), 3681−3686.
(45) Hillman, A. R.; Skopek, M. A.; Gurman, S. J. X-Ray Spectroscopy of Electrochemically Deposited Iridium Oxide Films: Detection of Multiple Sites through Structural Disorder. *Phys. Chem. Chem. Phys.* **2011**, *13* (12), 5252−5263.
(46) Gao, J.; Xu, C. Q.; Hung, S. F.; Liu, W.; Cai, W.; Zeng, Z.; Jia, C.; Chen, H. M.; Xiao, H.; Li, J.; Huang, Y.; Liu, B. Breaking Long-Range Order in Iridium Oxide by Alkali Ion for Efficient Water Oxidation. *J. Am. Chem. Soc.* **2019**, *141* (7), 3014−3023.
(47) Shannon, R. D. Revised Effective Ionic Radii and Systematic Studies of Interatomic Distances in Halides and Chalcogenides. *Acta Crystallogr., Sect. A* **1976**, *32* (5), 751−767.
(48) Newville, M.; Stensitzki, T.; Allen, D. B.; Rawlik, M.; Ingargiola, A.; Nelson, A. *LMFIT: Non-Linear Least-Square Minimization and Curve-Fitting for Python*, version (0.8.0); Zenodo, 2016.
(49) Ravel, B.; Newville, M. ATHENA and ARTEMIS: Interactive Graphical Data Analysis Using IFEFFIT. *Phys. Scr.* **2005**, *2005*, 1007−1010.
(50) Newville, M. Larch: An Analysis Package for XAFS and Related Spectroscopies. *J. Phys. Conf. Ser.* **2013**, *430*, 012007.
(51) Choy, J. H.; Kim, D. K.; Hwang, S. H.; Demazeau, G.; Jung, D. Y. XANES and EXAFS Studies on the Ir−O Bond Covalency in Ionic Iridium Perovskites. *J. Am. Chem. Soc.* **1995**, *117* (33), 8557−8566.
(52) Ankudinov, A. L.; Ravel, B.; Rehr, J. J.; Conradson, S. D. Real-Space Multiple-Scattering Calculation and Interpretation of x-Ray-Absorption near-Edge Structure. *Phys. Rev. B* **1998**, *58* (12), 7565−7576.

https://doi.org/10.1021/acscatal.4c03562
ACS Catal. 2024, 14, 16759−16769